LONGITUDINAL COMPRESSIVE BEHAVIOUR OF CARBON FIBRES

N. Oya[1], D. J. Johnson[1], and H. Hamada[2]

[1] *School of Textile Industries, University of Leeds*
Leeds, West Yorkshire, LS2 9JT, UK
[2] *Advanced Fibro-Science, Kyoto Institute of Technology*
Matsugasaki, Sakyo-ku, Kyoto 606-8585, Japan

SUMMARY: Longitudinal compressive strengths of PAN-based carbon fibres were measured by a new direct measurement method; the results were correlated with microstructural parameters obtained from wide-angle X-ray scattering. Compressive strengths were found to be much lower than tensile strengths; they were independent of crystallite disorder and crystallite size for HS (high strength) fibres, but were dependent on porosity. However, compressive strengths changed in respect of crystallite disorder, size and porosity for HM (high modulus) fibres. From these compressive strength-structure relations, it was concluded that the high strengths of HS fibres have been achieved by low porosity, and that the high moduli of HM fibres have been obtained by reduced disorder and larger crystallites, which have also led to a few large pores. The compressive strengths of HM fibres are lower than those of HS fibres.

KEYWORDS: carbon fibre, compression, stress, modulus, scanning electron microscope (SEM), X-ray diffraction, microstructure, CFRP

INTRODUCTION

It is generally accepted that carbon fibre reinforced plastics (CFRP) show poor compressive properties along the fibre axis, despite the superior tensile properties [1, 2]. Such a difference in compression and tension is undoubtedly associated with the unique micro-structure of carbon fibres. Structural characterisation by X-ray diffraction has revealed that the structure basically consists of stacking layers of highly oriented graphite planes including some disordered regions and microvoids. Poor longitudinal compressive properties of carbon fibres may be attributed to such highly oriented crystallite structures. However, longitudinal compressive properties of carbon fibres are difficult to measure and have not been properly correlated with structural parameters. The compressive property-structure relationship in carbon fibres must be established at single filament level in order to improve the mechanical performance of CFRP in any particular end use.

For many years, researchers have endeavoured to find appropriate compression test methods; those which have been used include the elastica loop method [3], the bending beam method

[4], the single-fibre composite method [5], and the tensile-recoil method [6]. Together, these methods have provided much useful information for comparisons of fibre compressive properties; however, all four have vital drawbacks because of their indirect interpretations of compressive properties. The tensile-recoil technique is often applied because of the relatively easy testing procedure. In this method, a fibre sample is stretched to a predetermined tensile stress level and a recoil compressive effect is initiated by severing the sample at the midpoint. The recoil compressive stress which is equivalent to the released tensile stress takes place along the sample and propagates towards both ends. If the recoil stress exceeds the compressive strength of the sample, a compressive failure occurs. The critical compressive strength with 50% failure probability may be determined by testing several specimens with various initial tensile stress levels. However, the method has some problems, particularly with respect to dynamic loading and specimen buckling [7-10].

This paper describes an original development of a novel method for longitudinal compressive strengths of single carbon fibres. The results will be compared to those from the recoil method. The compressive strength-structure relationship will be revealed with the aid of structural characterisation by wide-angle X-ray scattering (WAXS).

EXPERIMENTAL

Samples

Seven kinds of polyacrylonitrile- (PAN-) based fibres manufactured by Toray Industries, Inc. were used for studying longitudinal compressive behaviour and microstructures of carbon fibres. Relevant mechanical and physical properties of the fibres are listed in Table 1. They are typically classified into two categories; high strength (HS) and high modulus (HM). T fibres (T300, T700S, T800H and T1000) are regarded as the HS fibres, MJ fibres (M40J, M50J and M60J) are HM fibres and designated according to each modulus level.

Table 1: Mechanical and physical properties of PAN-based carbon fibres.

	Diameter*1 (μm)	Tensile strength*2 (GPa)	Tensile modulus*2 (GPa)	Strain-to-failure (%)	Density*3 (g/cm^3)
T300	7.01	3.5	210	1.68	1.75
T700S	6.75	5.3	237	2.23	1.82
T800H	4.97	6.4	306	2.19	1.81
T1000	5.00	7.1	294	2.40	1.82
M40J	5.21	4.9	335	1.45	1.77
M50J	5.19	4.3	430	1.00	1.88
M60J	5.07	3.5	535	0.65	1.94

*1 Fibre diameter measured by SEM assuming a circular cross section.
*2 Tensile properties based on ASTM D-3379.
*3 Density supplied by the manufacturer.

It is not clear as to the conditions under which these fibres were prepared as they are considered to be of a proprietary nature but, most probably, HM fibres experienced temperatures up to and above 2773K and HS fibres 1573K.

Single fibre compression test

Longitudinal compressive properties of carbon fibres were measured as follows. Firstly, a carbon filament sample was carefully cut at one end with a razor blade to prepare a flat-end column specimen. The sample was then vertically glued on to one edge of a brass stage with instant glue. The portion sticking out from the edge was regarded as the gauge length, which was adjustable from 20 to 500μm with the aid of a light microscope.

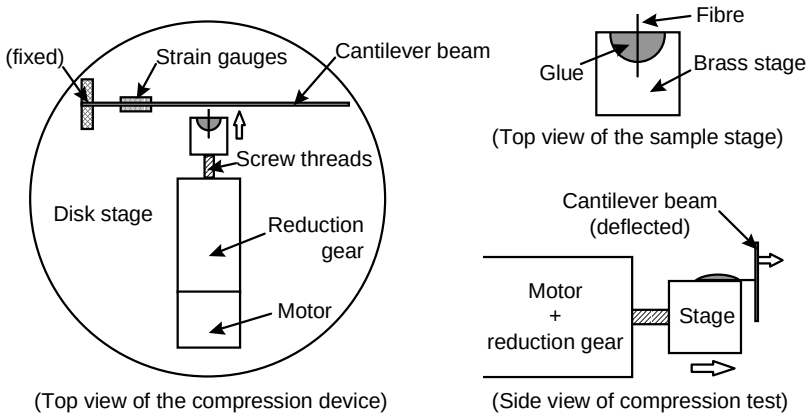

Fig. 1: Compression device for single carbon fibre.

As shown in Fig. 1, the brass sample stage was set on to micrometer screw threads in a DC motor assembly placed on a 7cm diameter aluminium disk, and mechanically driven at a constant speed of 0.13μm/sec. As the motor rotated, the filament sample was eventually compressed between the brass stage and a steel cantilever beam. The off-axis effect from the cantilever was negligible because of the very small deflection compared to the length of the cantilever beam. Semiconductor strain gauges detected a signal when the cantilever beam was deflected by the fibre. The signal was amplified and then converted to force according to a prior calibration for the strain gauges. The data was stored digitally in a PC and a force-time curve plotted on the screen during the test. Longitudinal compressive strength was calculated by dividing the ultimate force by the cross-sectional area of the sample.

Typical stress-time curves at different specimen gauge lengths are shown in Fig. 2. The compressive stress linearly increased until the final fracture at short specimen gauge lengths, whereas buckling behaviour was clearly seen at long gauge lengths. Longitudinal compressive strength was estimated at non-buckling gauge lengths from an average value of at least 20 readings for each fibre.

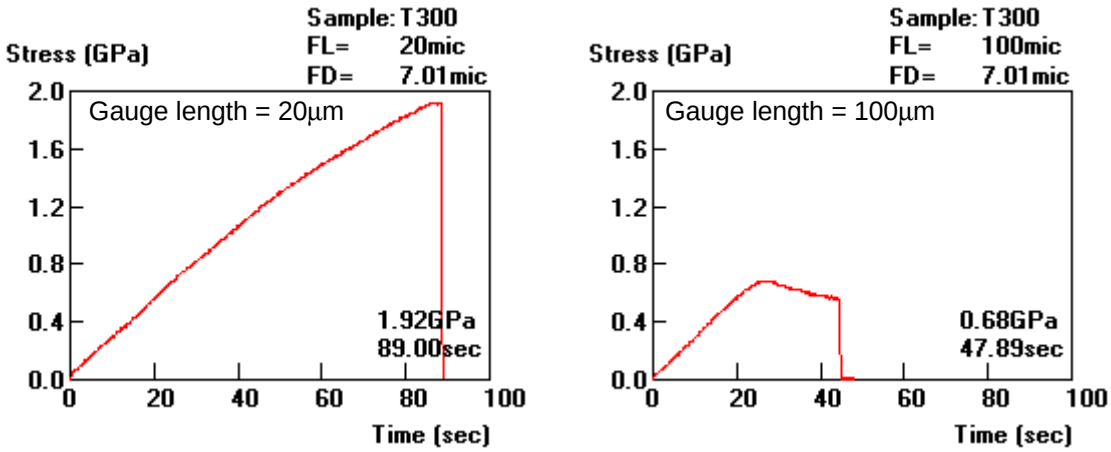

Fig. 2: Stress-time curves at different gauge lengths.

The compressive behaviour of each sample can be observed either by a light microscope or a scanning electron microscope (SEM). Before the in-situ SEM observation, the sample was coated by a thin gold layer of 20nm thickness.

Wide angle X-ray scattering (WAXS)

X-ray diffraction traces of aligned fibres were recorded using a position-sensitive detector (PSD) with CuKα radiation (λ = 1.540598Å) operating at 40kV and 16mA. The diffraction pattern was normalised, corrected and peaks resolved using standard computational methods adapted for PC analysis [11]. The interlayer spacing d_{002} and the crystallite size in the *c*-axis direction L_c were estimated from the position and half-height width of the resolved 002 reflection, position being calibrated from standard silver peak positions. The crystallite sizes in the *a*-axis directions, $L_{a//}$ and $L_{a\perp}$, were determined from the 100 reflections on the meridian and equator, respectively.

As a measure of disorder, the relative degree of intracrystallite imperfection D_c was calculated from the relation

$$D_c = \left[1 - \frac{d_{turb} - d_{obs}}{d_{turb} - d_{gra}}\right] \times 100 \qquad (1)$$

where d_{turb}, d_{gra} and d_{obs} are the interlayer spacings d_{002} in a turbostratic carbon, perfect graphite and the actual carbon fibre, respectively (d_{turb} = 0.350nm and d_{gra} = 0.335nm).

The micro-porosity was estimated as follows [12]. The X-ray density ρ_x was calculated using

$$\rho_x = (3.33538 / d_{002}) \times 2.268\text{g/cm}^3 \qquad (2)$$

where 3.33538 is d_{002} and 2.268g/cm^3 is ρ_x of pure graphite.

The total pore volume is defined as

$$\text{total pore volume} = (1 / \rho_g - 1 / \rho_x) \qquad (3)$$

where ρ_g is the density of actual fibre. Total % porosity *p* is then calculated from

$$p = \text{total pore volume} \times \rho_g \times 100. \qquad (4)$$

RESULTS AND DISCUSSION

Longitudinal compressive properties

Longitudinal compressive strength of each PAN-based carbon fibre was estimated at short gauge length to avoid any buckling effect as described earlier. Fig. 3 compares the longitudinal compressive strength obtained from our direct method and the conventional recoil technique. It was difficult to obtain the direct strength for T1000, because buckling deformation was evident even at a gauge length of 20μm, the shortest length possible to test

with this method. Therefore, it must be noted that the strength was indicated as more than 2.8GPa.

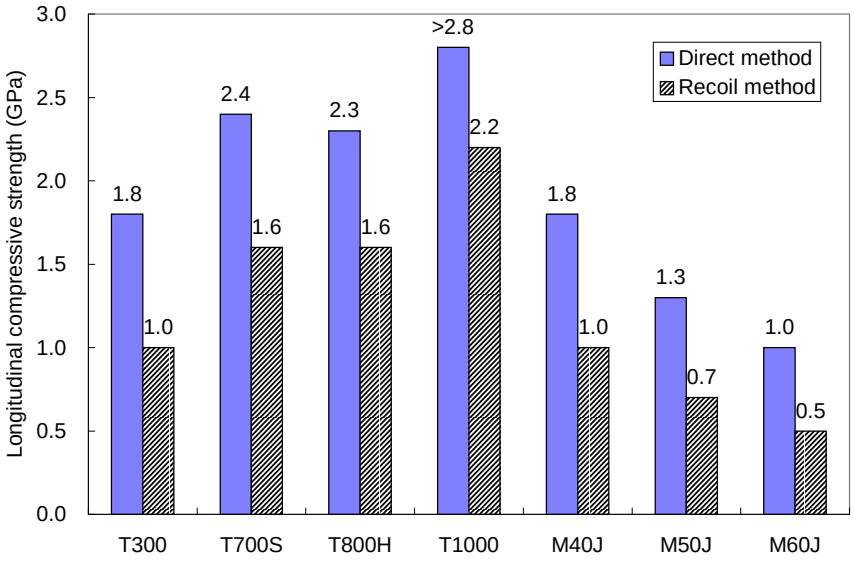

Fig. 3: Comparison of direct and recoil compressive strength.

It is clear that in general the direct strength was higher for each fibre. It is likely that the recoil technique underestimates the strength due to the intrinsic dynamic impact and buckling of long specimens.

Fig. 4 compares the longitudinal compressive and tensile strengths. The compressive strengths were definitely lower; from one-third to one-half of the tensile strengths. It was also confirmed that the compressive strengths improved with increase of the tensile strengths. However, the improvement of tensile strength was much more efficient, especially for HS fibres, than that of compressive strength. This may be reflected by the fact that the highly oriented structure is more convenient to improve the tensile properties.

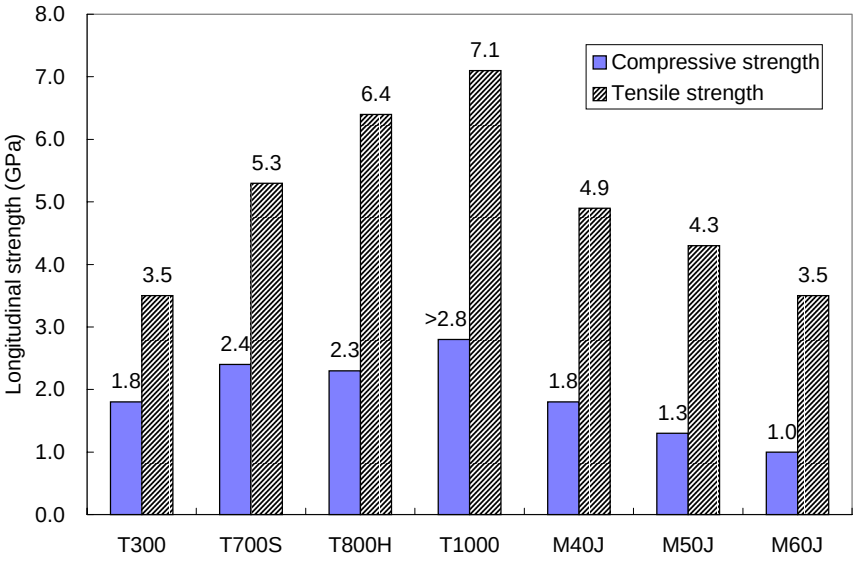

Fig. 4: Comparison of compressive and tensile strength.

In-situ SEM observations were also attempted in this study. For HS fibres, there was no significant surface change during compression until catastrophic failure. On the contrary, for HM fibres (particularly for M60J), kink bands appeared on the surface as shown in Fig. 5 (a) and (b). Subsequently, as shown in Fig. 5 (c) and (d), the kink bands always developed into splitting failure along the fibre axis. Such surface changes strongly suggest local buckling of crystallites due to large needle-like pores, as discussed in the following section.

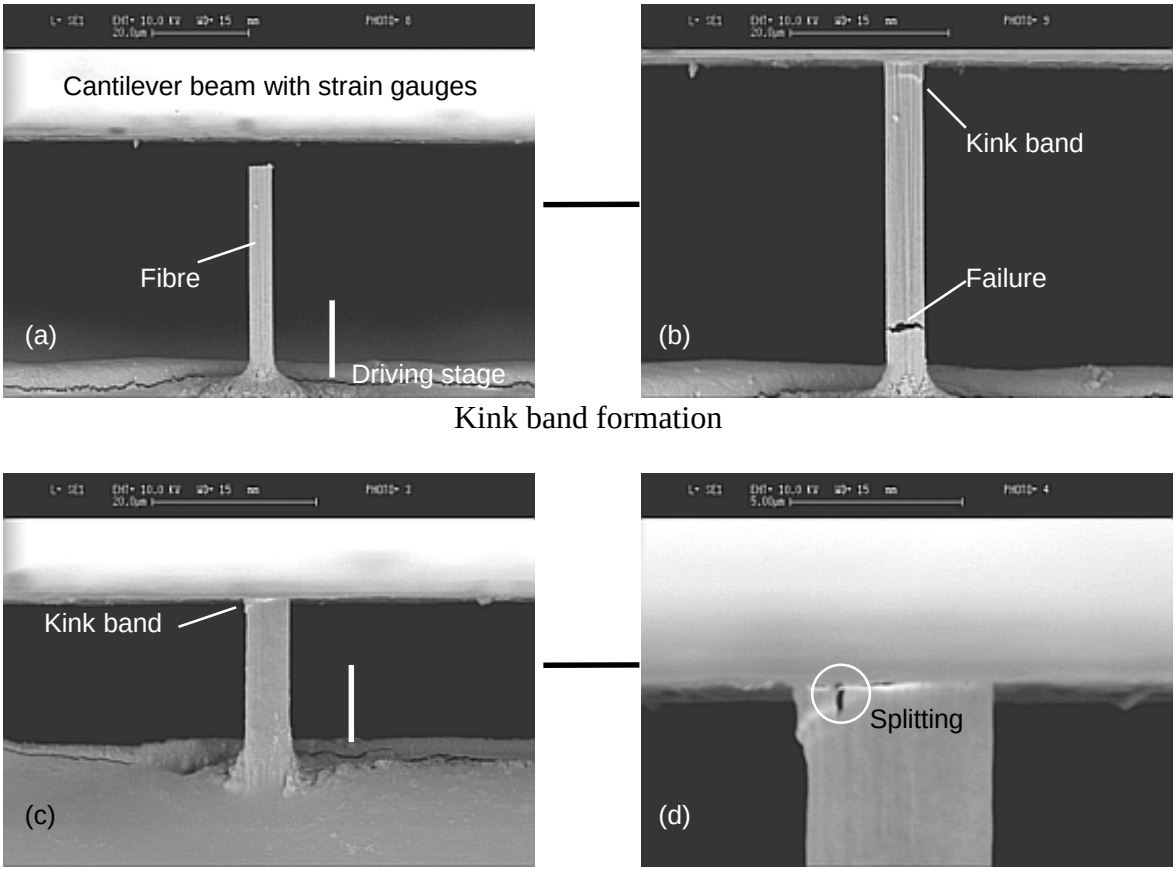

Kink band formation

Post-kink splitting

Fig. 5: In-situ SEM observations for HM fibre (M60J).

Microstructure

Table 2 lists the structural parameters obtained from wide-angle X-ray scattering. Interlayer spacing d_{002} and intracrystallite disorder D_c showed the same values for all HS fibres. On the other hand, both values declined with increase of modulus level for HM fibres. Crystallite sizes in three directions (L_c, $L_{a\perp}$ and L_{all}) also exhibited similar trends; no size changes for HS fibres and significant increase for HM fibres. These results show that the crystallite structure of HM fibre approaches that of perfect graphite with increasing modulus.

As regards total % porosity p, T300 showed the highest value among HS fibres. For HM fibres, the porosity decreased with increase of modulus. From these measurements, it was found that HS fibres had only structural difference in the porosity, whereas HM fibres had difference in respect of disorder, crystallite size, and porosity.

Table 2: Structural parameters from wide-angle X-ray scattering.

	d_{002} (nm)	D_c (%)	L_c (nm)	$L_{a\perp}$ (nm)	L_{all} (nm)	p (%)
T300	0.347	80.0	2.26	4.39	2.38	19.7
T700S	0.347	80.0	2.26	4.38	2.38	16.5
T800H	0.347	80.0	2.26	4.39	2.38	17.0
T1000	0.347	80.0	2.26	4.38	2.38	16.5
M40J	0.342	46.7	3.51	6.28	5.42	19.9
M50J	0.340	33.3	5.48	7.91	7.51	15.3
M60J	0.339	26.7	8.40	8.91	8.76	13.0

Compressive property-structure relations in carbon fibres

Compressive strength and disorder region

Fig. 6 shows the relationship between longitudinal compressive strength and intracrystallite disorder D_c. Compressive strengths were independent of crystallite disorder for HS fibres. However, there was a proportional relationship for HM fibres; the more the disorder, the higher the compressive strength.

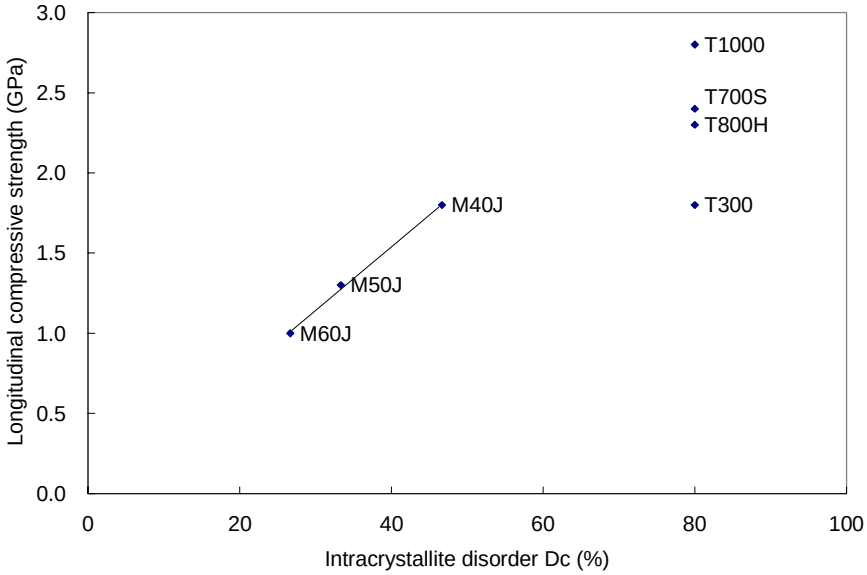

Fig. 6: Longitudinal compressive strength vs intracrystallite disorder.

Compressive strength and crystallite sizes

Fig. 7 shows the relationship between longitudinal compressive strength and crystallite size L_c. The relationship was similar to the case of intracrystallite disorder; compressive strengths were independent of crystallite size for HS fibres and dependent for HM fibres. Similar relations were obtained for $L_{a\perp}$ and L_{all}. Larger crystallites contributed to lower compressive strength and higher modulus for HM fibres.

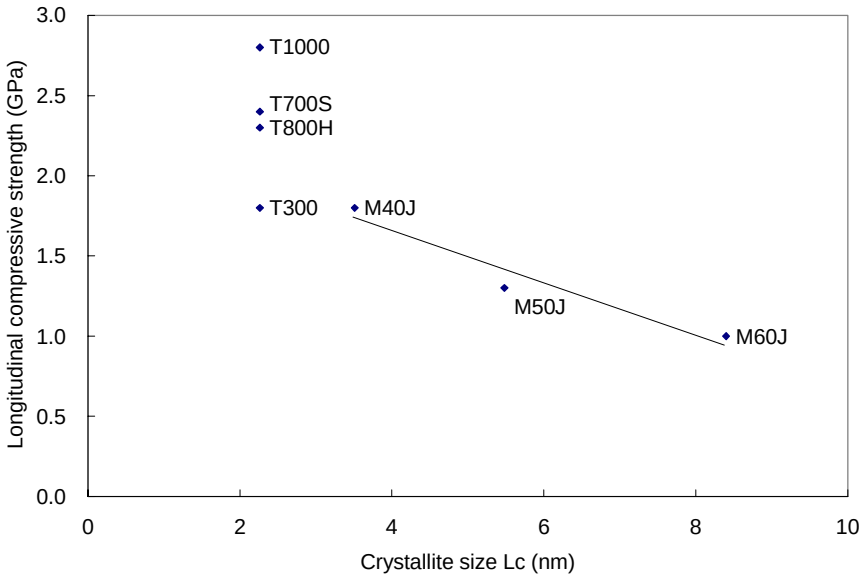

Fig. 7: Longitudinal compressive strength vs crystallite size L_c.

Compressive strength and porosity

Fig. 8 shows the relationship between longitudinal compressive strength and total % porosity *p*. It can be seen that compressive strength decreased with increase of porosity for HS fibres. On the contrary, compressive strength increased with increasing porosity for HM fibres.

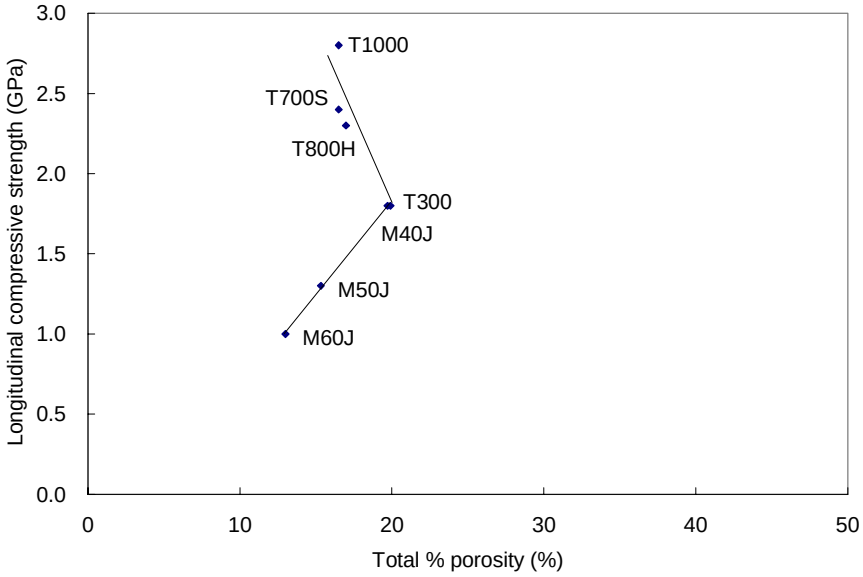

Fig. 8: Longitudinal compressive strength vs total % porosity.

Considering the fact that the strength was independent of disorder and crystallite size for HS fibres, it can be explained that the high strengths of these fibres have been achieved by diminishing microvoids with carefully controlled manufacturing process.

On the other hand, HM fibres showed the reverse relationship, in which the strength became lower with less porosity. This contradiction can be explained from different types of pores in HS and HM fibres. HM fibres have been provided with high moduli resulting from higher heat treatment temperatures (HTT). Such high HTT and high modulus generally results in a

system change from many small pores to a few large needle-like pores. The low porosity is probably reflected by presence of fewer large pores for HM fibres. Small-angle X-ray scattering (SAXS) work has reported such coalesced pores in high modulus carbon fibres supported by increasing cross-sectional area and decreasing number of voids crossing unit area of a plane perpendicular to the fibre axis [12]. Accordingly, for HM fibres used in this study, it is thought that the longitudinal compressive strength was sacrificed because of the large needle-like pores. This is supported by in-situ SEM micrographs of M60J which showed surface kink bands and post-kink splitting most probably originating from buckling of large crystallites adjacent to large needle-like pores.

From the compressive strength-structure relations obtained in this study, some basic remarks on the manufacturing process of carbon fibres can be made. In order to maximise the compressive properties of PAN-based carbon fibres, it is very important to control the microporosity especially for high compressive strength. High modulus can be attained by reducing the disorder regions and enlarging the crystallite sizes, however, care must be taken to minimise the occurrence of large needle-like pores.

CONCLUSIONS

Longitudinal compressive strengths of PAN-based carbon fibres were successfully measured by a new direct method. Results were generally higher than those from the conventional tensile-recoil test. The lower recoil strengths were probably due to the intrinsic dynamic impact and buckling of long specimens in this method.

Compressive strength was found to be considerably lower than tensile strength for each fibre; about one-third to one-half of the tensile strength. The compressive strength improved with increase of tensile strength, however, the improvement was much more efficient in the tensile strength. Such a difference in tension and compression is reflected by the intrinsic nature of carbon fibre structures.

Longitudinal compressive strength-microstructure relations were quantitatively discussed with the aid of wide-angle X-ray scattering. Compressive strengths of HS fibres were only dependent on the microporosity. HM fibres showed high moduli due to fewer disordered regions and larger crystallite sizes. However, compressive strengths of those fibres were sacrificed by presence of fewer but larger pores.

In order to maximise the compressive properties of PAN-based carbon fibres, it is very important to control the microporosity especially for high compressive strength. High modulus can be attained by reducing disorder and enlarging the crystallite size, however, care must be taken to minimise the occurrence of large needle-like pores.

ACKNOWLEDGEMENTS

The financial support of an Overseas Research Student (ORS) Scholarship and a Tetley and Lupton Scholarship from Her Majesty’s Government (UK) and the University of Leeds are gratefully acknowledged by N. O. The authors wish to thank Mr. N. Takada and H. Suzue of Daiwa Seiko, Inc. for providing the carbon fibres used in this study.

REFERENCES

[1] N.OYA and H.HAMADA, *Journal of Science and Engineering of Composite Materials*, vol.5, no.3-4, 1996, p.105.

[2] N.OYA and H.HAMADA, *Composites* Part A **28A** (1997) 823.

[3] D. SINCLAIR, *J. Appl. Phys.* **21** (1950) 380.

[4] S. J. DETERESA, S. R. ALLEN, R. J. FARRIS and R. S. PORTER, *J. Mater. Sci.* **19** (1984) 57.

[5] H. M. HAWTHORNE and E. TEGHTSOONIAN, *J. Mater. Sci.* **10** (1975) 41.

[6] S. R. ALLEN, *J. Mater. Sci.* **22** (1987) 853.

[7] G. J. HAYES, D. D. EDIE and J. M. KENNEDY, *J. Mater. Sci.* **28** (1993) 3247.

[8] M. G. DOBB, D. J. JOHNSON and C. R. PARK, *J. Mater. Sci.* **25** (1990) 829.

[9] C. S. WANG, S. J. BAI and B. P. RICE, in "Proceedings of the American Chemical Society", Vol.61, Division of Polymeric Materials: Science and Engineering, Miami, FL, 1989 (ACS, 1989) p.550.

[10] M. FURUYAMA, M. HIGUCHI, K. KUBOMURA, H. SUNAGO, H. JIANG and S. KUMAR, *J. Mater. Sci.* **28** (1993) 1611.

[11] A. M. HINDELEH, D. J. JOHNSON and P. E. MONTAGUE, In *Fibre Diffraction Methods* (Edited by A. D. French and K. H. Gardner), p.149. American Chemical Society, Washington, DC (1983).

[12] A. GUPTA, I. R. HARRISON and J. LAHIJANI, *J. Appl. Cryst.* **27** (1994) 627.